# Mesenchymal Stem Cell Fates in Murine Acute Liver Injury and Chronic Liver Fibrosis Induced by Carbon Tetrachloride[S]

## Chenhui Ma, Li Han, Jiajun Wu, Feng Tang, Qiangqiang Deng, Ting He, Zhitao Wu, Chen Ma, Wei Huang, Ruimin Huang, and Guoyu Pan

*Shanghai Institute of Materia Medica, Chinese Academy of Sciences, Shanghai, China (C.M., L.H., J.W., F.T., Q.D., T.H., Z.W., C.M., W.H., R.H., G.P.); University of Chinese Academy of Sciences, Beijing, China (C.M., L.H., J.W., F.T., C.M., W.H., R.H., G.P.); and School of Pharmaceutical Sciences, Nanjing Tech University, Nanjing, China (T.H.)*

## ABSTRACT

Mesenchymal stem cells (MSCs) therapy has shown potential benefits in multiple diseases. However, their clinic performance is not as satisfactory as expected. This study aimed to provide an alternative explanation by comparing MSCs' fates in different liver diseases. The distribution and therapeutic effects of human MSC (hMSCs) were investigated in acute liver injury (ALI) and chronic liver fibrosis (CLF) mice models, respectively. The two models were induced by single or repeated injection of carbon tetrachloride separately. The increase of hMSCs exposure in the liver (AUC$_{liver\ 0-72\ hour}$) were more significant in ALI than in CLF (177.1% versus 96.2%). In the ALI model, the hMSCs exposures in the lung (AUC$_{lung\ 0-72\ hour}$) increased by nearly 50%, whereas it decreased by 60.7% in CLF. The efficacy satellite study indicated that hMSCs could significantly ameliorate liver injury in ALI, but its effects in CLF were limited. In the ALI, suppressed natural killer (NK) cell activities were observed, while NK cell activities were increased in CLF. The depletion of NK cells could increase hMSCs exposure in mice. For mice MSC (mMSCs), their cell fates in ALI were very similar to hMSCs in ALI: mMSCs' exposure in the liver and lung increased in ALI. In conclusion, our study revealed the distinct cell pharmacokinetic patterns of MSCs in ALI and CLF mice, which might be at least partially attributed to the different NK cell activities in the two liver diseases. This finding provided a novel insight into the varied MSCs' therapeutic efficacy in the clinic.

## SIGNIFICANCE STATEMENT

Currently, there is little knowledge about the PK behavior of cell products like MSCs. This study was the first time investigating the influence of liver diseases on cell fates and efficacies of MSCs and the underneath rationale. The exposure was distinct between two representative liver disease models, which directly linked with the therapeutic performance that MSCs achieved. The difference could be attributed to the NK cells–mediated MSCs clearance.

## Introduction

Mesenchymal stem cells (MSCs) have already exhibited great potency in multiple diseases. For example, MSCs exerted beneficial effects against graft-versus-host disease and were recommended as a second-line treatment option for acute graft-versus-host disease (Zhao et al., 2022). Besides, the survival rate of patients with hepatitis B-associated liver failure was significantly improved by human MSCs (hMSCs) (79.2%) compared with the control group (52.6%) during the first 12 weeks of follow up (Shi et al., 2012).

However, there are plenty of controversial reports about the clinical performance of MSCs, and the results are not as satisfactory as what has been achieved in preclinic animal studies (Daley, 2012; Xu et al., 2018). Many clinical trials found a substantial nonresponse rate and significant individual variabilities after MSCs treatment (Wysoczynski

et al., 2018; Zhao et al., 2018). For example, one study reported an improved survival rate and liver function after MSCs treatment in acute-on-chronic liver failure patients (Shi et al., 2012). In contrast, another study showed that MSCs couldn't benefit decompensated cirrhosis patients (Mohamadnejad et al., 2013). The inconsistency may be partly explained by the varied resources and derivation, the CMC quality, and clinic delivery routes. However, the variance of patients' immune systems and disease severity is a crucial but less recognized source of heterogeneity in cell therapy (Yang et al., 2020).

Previous studies indicated that most MSCs mainly distributed in the lung and liver and have limited engraftment capacity (Shim et al., 2015; Creane et al., 2017). However, whether the pharmacokinetic (PK) pattern of MSCs would be altered under diseases and the mechanism remains to be elucidated. Natural killer (NK) cells are innate immune cells endowed with the inherent ability to recognize and eliminate foreign and infected cells (Freud et al., 2017). Although activated natural killer cells were reported to facilitate MSCs lysis in vitro (Poggi et al., 2005), to our knowledge, there is no direct evidence linking NK cell function with MSCs therapeutic efficacy and disposition during liver diseases.

Given the efficacy instability and discrepancy observed among MSCs-related studies, our work aimed to find potential explanations by

**ABBREVIATIONS:** ALI, acute liver injury; ALT, alanine aminotransferase; AST, aspartate aminotransferase; CCl$_4$, carbon tetrachloride; CLF, chronic liver fibrosis; FU, fluorescent units; IVIS, in vivo imaging system; MSC, mesenchymal stem cell; NK, natural killer cells; PK, pharmacokinetics; qPCR, quantitative polymerase chain reaction.

investigating the fate of MSCs in two representative liver injury mice models: carbon tetrachloride ($CCl_4$)-induced acute liver injury (ALI) and $CCl_4$-induced chronic liver fibrosis (CLF). The PK behavior, the therapeutic performance, the role of NK cells-mediated clearance, and species difference would be systemically compared to explore the potential regulator of the pharmacokinetics (PK) and pharmacodynamics patterns of MSCs, a promising cell-based therapy.

## Materials and Methods

**Cells.** The human umbilical cord-derived mesenchymal stem cells (hMSCs) were kindly provided by Hexaell Biotech (Shanghai, China). The umbilical cord was collected from the informed consent mother, according to a protocol approved by the Institutional Ethical Review Committee of Sir Run Run Shaw Hospital, School of Medicine, Zhejiang University. MSCs were isolated according to a previous study (Han et al., 2013; Zhong et al., 2020). Briefly, umbilical cord tissues were cut and digested with collagenase IV (Sigma, St. Louis, MO) and Trypsin (Gibco, Carlsbad, CA). The cell pellet was then resuspended and cultured. hourMSCs were further expanded by changing the medium every two days. The culture medium was α-minimal essential medium (α-MEM, Gibco) with 10% fetal bovine serum (FBS) (Sigma) and 1% penicillin-streptomycin (P/S) (Gibco) and 1% L-glutamine (Gibco). The mice adipose-derived mesenchymal stem cells (mMSCs) were isolated from male Balb/c mice, as reported previously (Estes et al., 2010). mMSCs were cultured in Dulbecco's modified Eagle's medium (Hyclone, Logan, UT) with 10% FBS and 1% L-glutamine and 1% P/S. The hMSCs used in subsequent experiments were between passages three to seven. The mMSCs were used at passage two or three. The human cell line NK92 was obtained from the American Type Culture Collection (ATCC). NK92 cells were cultured in α-MEM (Gibco) supplemented with 25% FBS, 0.2 mM inositol (Sigma), 0.1 mM 2-mercaptoethanol (Sigma), 0.02 mM folic acid (Sigma), and 100 $U \cdot ml^{-1}$ recombinant human IL-2 (Peprotech, Rocky Hill, NJ). All cells were cultured in a humidified 5% $CO_2$, 95% air incubator at 37°C.

**Fluorescent Labeling to Detect the Biodistribution of MSCs.** The in vivo distribution of injected MSCs was monitored according to our previous paper (Han et al., 2021). Briefly, MSCs were harvested with 0.25% Trypsin (Gibco) and washed by PBS three times. Then, cell pellet was incubated with 10 μM Cy5-NHS (Meilunbio, China) in PBS (pH 8.0) at 37°C for 30 minutes. The reaction was terminated by adding 100 mM glycine and then washed with PBS three times. The pellet was then resuspended in a sterile PBS and subjected to intravenous injection. Mice were treated with 200 μl labeled hMSCs or mMSCs ($5 \times 10^5$ cells per mice). Mice were anesthetized with pentobarbital (50 mg·kg$^{-1}$) at indicated time points and sacrificed. Tissues (heart, liver, spleen, lung, and kidney) were collected and washed with sterile normal saline. The fluorescence of labeled MSCs in tissues was detected in an in vivo imaging system (IVIS) system (PerkinElmer, Waltham, MA) with a fixed exposure time (1 second) and filter setting of 640 nm excitation and 680 nm emission. Imaging analysis was performed using Living Image software (Caliper, Waltham, MA) to obtain the average radiance of each tissue. Fluorescent units (FU) mean the photons/s/cm$^2$/sr/μW/cm$^2$. FU were used to obtain the Fluorescence intensities-Time curve and PK parameters (see "Statistical Analysis").

**Detection of Human-Derived MSCs by Quantitative Real-Time PCR (qPCR).** About 10 mg of tissues were weighted for gDNA isolation using genomic DNA extraction kits (Magen, China). Quantitative real-time PCR (qPCR) was performed in a 20 μl total reaction volume containing 10 μl SYBR Green master mix (Yeason biotech, Shanghai, China), 200 ng of gDNA, and 1 μl forward and reverse primers in a 7500 Real-Time PCR system (ABI, Foster City, CA). The human-specific Alu primer and β-actin were listed in Supplemental Table 1. hourMSCs amounts in mice tissues were calculated according to the standard curve based on the logarithm of cell number and the CT value, according to our previous paper (Han et al., 2021).

**Animals.** All animal experiments were performed following the Ethical Treatment of Laboratory guidelines. The protocols involving animal experiments were reviewed and approved by the Institute of Animal Care and Use Committee of the Shanghai Institute of Material Medica, Chinese Academy of Sciences. Male Balb/c mice (6–8 weeks) were purchased from the Shanghai SLAC Laboratory Animal Co. (Shanghai, China). All animals were maintained under the

Specific-pathogen-free (SPF) condition with a constant temperature (23 ± 1.5°C) and humidity (55 ± 5%) on a 12-hour light and dark cycle.

**$CCl_4$-Induced Acute Liver Failure (ALI) in Mice.** To determine the efficacy and pharmacokinetics of MSCs in acute liver disease, the conventional $CCl_4$-induced ALI were employed. Balb/c mice were randomly divided into the following four groups ($n = 4–5$): control, hMSC, ALI, and hMSCs + ALI (Fig. 1A). The mice in the liver failure groups were intraperitoneally administered with 5 ml·kg$^{-1}$ of $CCl_4$ (Sinopharm, China) dissolved in olive oil (v/v, 20%, Sinopharm, China), whereas normal mice received solvent only as control. 6 hours after $CCl_4$ injection, $5 \times 10^5$ labeled MSCs diluted in 200 μl PBS or an equal volume of PBS were administered to mice via tail vein. Tissues were collected and imaged at 1, 8, 24, 48, and 72 hours after MSCs treatment to detect the biodistribution using IVIS. Liver, lung, and blood samples were also collected at 72 hours for histologic and biochemical analysis.

**$CCl_4$-Induced Chronic Liver Fibrosis (CLF) in Mice.** To investigate the potential different pharmacokinetic properties of MSCs in acute and chronic liver diseases, multiple doses of $CCl_4$ were administrated to induce liver fibrosis (Fig. 1E). Briefly, mice were randomly divided into four groups: control, hMSCs, fibrosis, and hMSCs + fibrosis. Mice received 20% $CCl_4$ (dissolved in olive oil, 5 ml·kg$^{-1}$, *i.p.*) or vehicle twice a week as previous described (Ye et al., 2019).

To evaluate the protective effect against fibrosis, hMSCs ($5 \times 10^5$ cells per mice) or PBS were injected into mice ($n = 3–4$) at 6 hours after the final administration of $CCl_4$ on the sixth week of the fibrosis model. 72 hours after hMSCs transplantation, mice were anesthetized and sacrificed, and serum, liver, and lung samples were harvested and maintained for further analysis.

To examine the biodistribution in advanced fibrosis, remaining mice ($n = 5$) received hMSCs ($5 \times 10^5$ cells per mice, i.v.) or PBS after the last $CCl_4$ injection on the eighth week. Mice were sacrificed and tissue samples were collected for IVIS examination at 1, 8, 24, 48, and 72 hours after hMSCs administration.

**NK Depletion in Mice.** To validate the role of NK cells in the elimination of MSCs, the NK cells were temporally depleted in vivo by intraperitoneal injection of 25 μl anti-asialo GM-1 antibody (Biolegend, San Diego, CA) 48 hours before the hMSCs administration. Then, the fluorescence intensities in tissues were detected at 1, 8, 24, and 48 hours using the IVIS system.

**Immunohistochemistry.** Mouse liver and lung fixed with 4% paraformaldehyde were embedded in paraffin. 4 μm tissue sections were sliced, followed by hematoxylin and eosin (H and E), according to standard protocol. Images of stained slices were visualized and captured by NanoZoomer S210 (Hamamatsu, Japan). For liver fibrosis analysis, 4-μm-thick liver sections were stained with Sirius red for collagen deposition and immunohistochemical staining for α-smooth muscle actin (α-SMA) (Abcam, Cambridge, MA). ImageJ Fiji (Schindelin et al., 2012) software was used to assess the area positive stained for Sirius-red staining and α-SMA protein expression at ×20 magnification. The area percentage from five randomly selected fields were counted and subjected to further statistical analysis.

**Biochemical Analysis.** Serum alanine aminotransferase (ALT) and aspartate aminotransferase (AST) levels were measured using commercial kits following the manufacturer's instructions (Nanjing JianCheng, China).

**Western Blot.** Protein samples were extracted from about 10 mg of frozen liver or lung by incubating with RIPA lysis buffer (Beyotime, China) supplemented with 1% proteinase cocktail (Sigma) on ice. Protein quantification was performed by the BCA Protein Assay Kit (Beyotime, China). Protein samples in sodium dodecyl sulfate (SDS, Meilunbio) buffer was heated to 95°C for 10 minutes and separated on SDS-polyacrylamide gels. Resolved proteins were then transferred onto PVDF (Polyvinylidene fluoride) membranes (Millipore, USA) and blocked with 5% milk in TBST (Tween-TBS buffer). The respective samples were probed with antibodies overnight at 4°C against primary antibodies: anticollagen 1a1 polyclonal antibody (1:1000, Proteintech, Chicago, IL), anti-α-SMA polyclonal antibody (1:1000, Proteintech) and anti-GAPDH polyclonal antibody (1:1000, Proteintech). Membranes were washed three times and then incubated for 1 hour at room temperature with HRP-conjugated anti-rabbit IgG (1:5000, Yeason biotech) and visualized by Pierce ECL Western Blotting Substrate (Thermo Fisher, Waltham, MA) in the CLINX ChemiScope 3300 mini system (Shanghai, China). The intensity of each band was determined using ImageJ software (National Institutes of Health, Bethesda, MD).

**RNA Extraction and qPCR Analysis.** Total RNA was extracted from about 10 mg of liver or lung using TRIzol reagent (Life Technology, Waltham,
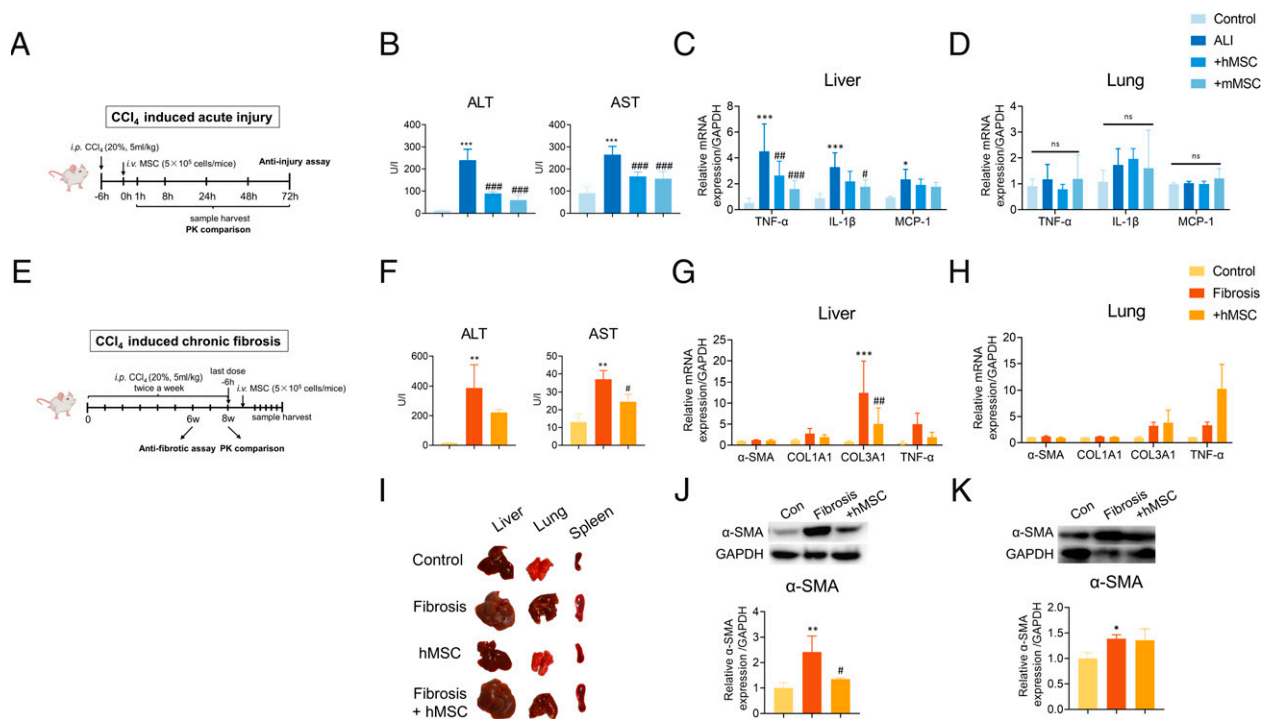
**Fig. 1.** hourMSCs and mMSCs could significantly ameliorate CCl₄-induced ALI but hMSCs showed limited antifibrotic effects in CLF mice. (A) Schematic illustration of the CCl4-induced acute liver injury experimental design. (B) Serum ALT, AST levels at 72 hours after hMSCs or mMSCs transplantation to CCl4-induced acute liver injury mice. (C–D) Hepatic and pulmonary mRNA expression of proinflammatory cytokines (TNF-α, IL-1β, and MCP-1). Data are shown as the mean ± S.D. ($n$ = 3–5 per group, *$P < 0.05$, ***$P < 0.001$, versus Con; #$P < 0.05$, ##$P < 0.01$, ###$P < 0.001$ versus ALI; ns, not significant). (E) Schematic illustration of the CCl4-induced chronic liver fibrosis experimental design. (F) Serum ALT and AST level at 72 hours after hMSCs injection to CCl4-induced chronic fibrosis mice. (G–H) qPCR analysis of the mRNA expression of α-SMA, Col1a1, Col3a1, TNF-α genes in liver and lung treated with hMSCs. (I) Gross examination showed enlargements of the liver, lung, and spleen in mice from the CLF model. (J–K) Relative α-SMA protein expression in the liver and lung from the CLF model were detected by western blot. Data are shown as the mean ± S.D. ($n$ = 3–5, *$P < 0.05$, **$P < 0.01$, ***$P < 0.001$, versus Con; #$P < 0.05$, ##$P < 0.01$, versus ALI or fibrosis; ns, not significant).

MA) and UNIQ-10 RNA RN column and collection tubes (Sangon Biotech, China). 1 ug of total RNA was used as a template for reverse transcription with 5×RT Master Mix (Takara, Japan), followed by qPCR detection with SYBR Green and primers as described above. Relative mRNA expression was normalized to the level of GAPDH and calculated using the $2^{-\Delta\Delta CT}$ method. Primers were designed and listed as shown in Supplemental Table1.

**Flow Cytometry.** The cell suspension was prepared by the digestion of fresh tissues (∼30 mg of liver, ∼10 mg of lung or spleens) in 1.5 mg·ml⁻¹ Collagenase Type I (to digest lung, Sigma) or Type IV (to digest liver and spleen, Sigma) dissolved in Roswell Park Memorial Institute 1640 medium (RPMI 1640, Meilunbio) at 37°C, 200 rpm for 1 hour. Single cells were then obtained by filtering and removing red blood cells by a Red Blood lysis buffer (Beyotime, China). Lymphocytes in blood were isolated using the Lymphocyte separation kit (Dakewe, China). The proportion of CD49b+Nkp46 cells was determined using anti-Nkp46 and anti-CD49b antibodies (Biolegend). All the staining processes were conducted based on the manufacturer's protocol, and then stained cells were detected by ACEA NovoCyte 3000 flow cytometer (Agilent, Santa Clara, CA). Data were analyzed using the FlowJo software (version 7.6).

**Immunofluorescence (IF) Staining.** Fresh liver and lung specimens were embedded in the OCT compound (SAKURA, USA) and stored at −80°C. The frozen samples were sectioned using a cryotome (Leica CM1850, Germany), and 5 μm-thick sections were fixed in 4% formaldehyde (Meilunbio). The sections were stained with rat anti-Nkp46 antibody (1:50, Biolegend) and goat anti-CD107a (1:50, R&D System, Minneapolis, MN) at 4°C overnight and then incubated with Alexa Fluor 594 Donkey Anti-Rat IgG (H+L) (1:300, Yeason biotech) and Alexa Fluor488 Donkey antigoat IgG (1:500, Abcam) for 1 hour. The slices were finally visualized with 4′,6-diamidino-2-phenylindole (DAPI) for nuclear staining. Images were digitalized using a fluorescence microscope (Echo, San Diego, CA).

**Cytotoxicity Assay.** The LDH assay was applied to detect the cytotoxicity as previously reported (Gotherstrom et al., 2011). NK92 cells were pretreated with a series of concentrations of human IL-2 for 72 hours and hMSCs were seeded at 2 × 10⁵ cells·ml⁻¹ 24 hours before assay. Then, the effector cells (NK92) were added to the hMSC wells at 30:1 (E:T ratio) and cocultured at 37°C for 4 hours. The LDH release was performed as the instruction mentioned (Dojinjo, Japan). After incubation, 20 μl of lysis buffer was added to the Positive Control (Pos) wells or 20 μl medium to the test wells and incubated at 37° C for 4 hours. The plate was centrifuged at 250 × g for 2 minutes and 100 μl of supernatant was transferred to a new 96-well plate. The reaction was induced by adding a working solution and stopped by a stop solution. The absorbance was measured at 490 nm by a microplate reader (BioTek, Winooski, VT). Cell cytotoxicity% was calculated according to the manufacturer's protocol, whereas the cytotoxicity% of the Pos group was set at 100%.

**Statistical Analysis.** All data were analyzed by GraphPad Prism software (version 8.0, GraphPad software, San Diego, CA) via one-way or two-way ANOVA, followed by Tukey's post hoc test for multiple comparisons between groups. The data are expressed as the mean ± S.D. $P < 0.05$ was considered statistically significant. The pharmacokinetic parameters were calculated by noncompartmental analysis with WinNonlin software (version 6.2; Pharsight, NC). The peak concentration ($C_{max}$), the peak time ($T_{max}$), the area under the concentration-time curve (AUC), elimination half-life($t_{1/2}$), and mean residence time (MRT) were determined separately.

## Results

**hMSCs Significantly Ameliorated Liver Inflammation in CCl₄-Induced Acute Liver Injury but Had Limited Effects against CCl₄-Induced Chronic Liver Fibrosis.** In this study, two representative liver disease models, acute liver injury (ALI), and chronic liver fibrosis (CLF) were induced respectively and the therapeutic performance hMSCs achieved in the two disease models were comprehensively investigated.
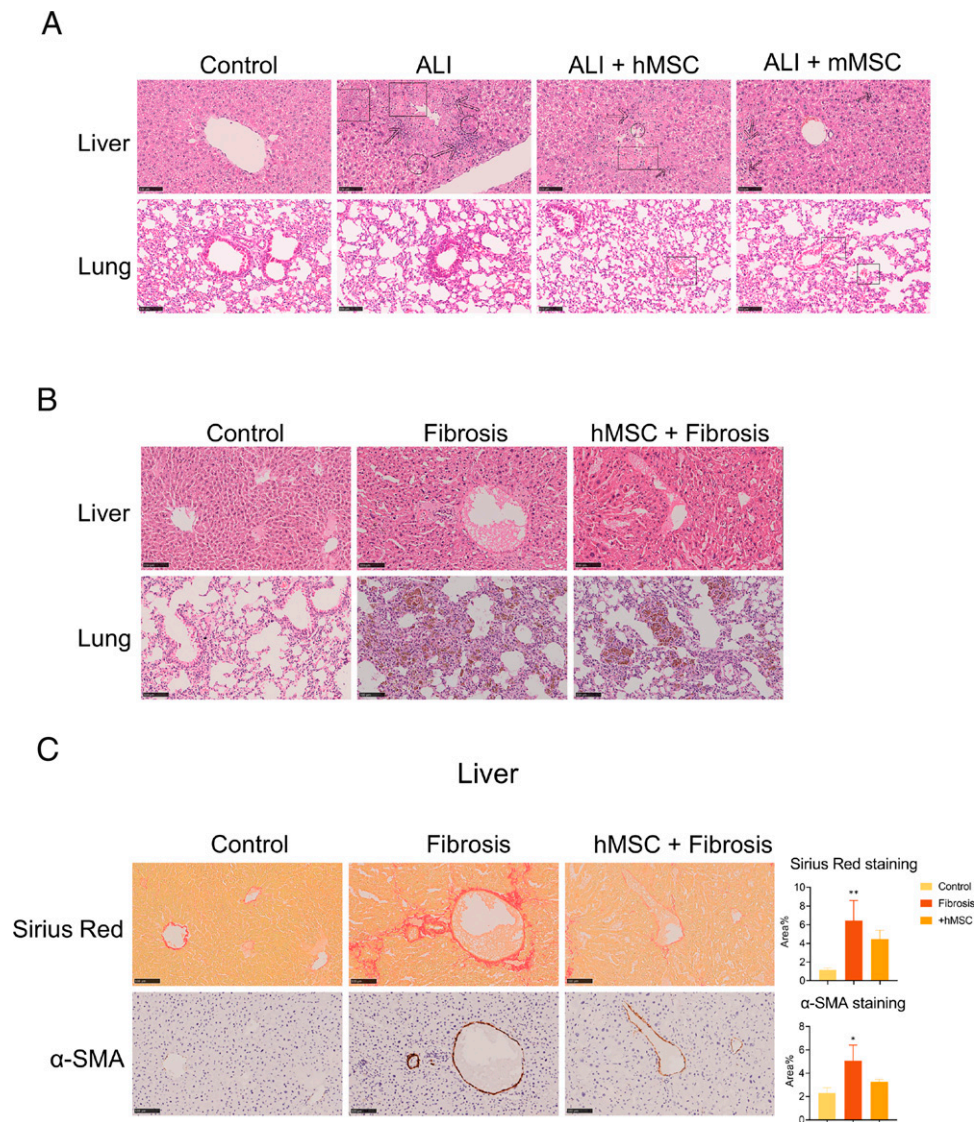
**Fig. 2.** Histologic examination of liver and lung. (A) Representative histologic photo of liver and lung in H and E staining in the ALI model. Scale bar: 100 $\mu$m. Symbols: black arrow, inflammation infiltration; rectangle, hemorrhage; circle, degeneration and necrosis. (B) Representative images of liver and lung H and E staining in CLF model. (C) Liver histologic sections from each group were subjected to Sirius red staining, IHC staining for $\alpha$-SMA and quantification analysis of Sirius red and $\alpha$-SMA positive area. Collagen was detected by Sirius red positive staining. Scale bar: 100 $\mu$m. Data are shown as the mean $\pm$ S.D. ($n = 3$, *$P < 0.05$, **$P < 0.01$, versus Con).

In the ALI experiment, a single dose of $CCl_4$ was intraperitoneally injected into Balb/c mice at 6 hours before labeled hMSCs or mMSCs ($5 \times 10^5$ cells per animal) transplantation (Fig. 1A). The elevated serum ALT/AST levels were significantly lowered in both hMSCs and mMSCs groups (Fig. 1B). mMSCs treatment worked better in ameliorating the increased proinflammatory genes (TNF-$\alpha$, IL-1$\beta$, and MCP-1) expression in the mice liver (Fig. 1C). Typical histopathological patterns of ALI were also observed in the injured liver, including severe hepatic necrosis, inflammatory cell infiltration, and hemorrhage (Fig. 2A). Hepatic necrosis and inflammation were improved on day 3 after MSCs administration. No significant histologic changes were observed in the murine lung after receiving MSC treatment (Fig. 2A), neither did the changes of the proinflammatory gene expressions (Fig. 1D).

To induce chronic liver fibrosis, mice receive repeated administration of $CCl_4$ (Fig. 1E). The effect of intravenously injected hMSCs ($5 \times 10^5$ cells per animal) against liver fibrosis was examined after the last administration of $CCl_4$ on day 42 (end of the sixth week).

Gross examination showed enlargements of the liver, lung, and spleen, rougher and harder liver, and obvious pulmonary congestion in fibrosis mice (Fig. 1I). hourMSCs could reduce serum ALT/AST levels and hepatic profibrotic gene and $\alpha$-SMA protein expressions (Fig. 1, F–G, L, and J). H and E, Sirius red staining (for collagen) and $\alpha$-SMA (biomarker of myofibroblast) expression all indicated that collagen deposition and inflammatory cell infiltration occurred in the fibrotic liver (Fig. 2, B and C). After hMSC treatment, hepatic histologic examination showed some extent of improvement, but the data were not statistically significant (Fig. 2, B and C).

According to previous studies, chronic interstitial pneumonia and intra-alveolar fibrosis could be observed during long-term administration of $CCl_4$ (Paakko et al., 1996; Taslidere et al., 2014). The pathology of lung tissues was also investigated. The increased expression of Col3a1 and TNF-$\alpha$ genes and $\alpha$-SMA were observed in fibrosis mice (Fig. 1, H and K). The results suggested a single hMSCs injection could not reverse the pathologic damage in the lung in CLF animals (Fig. 2B), but it may improve the animal condition and delay fibrosis development.
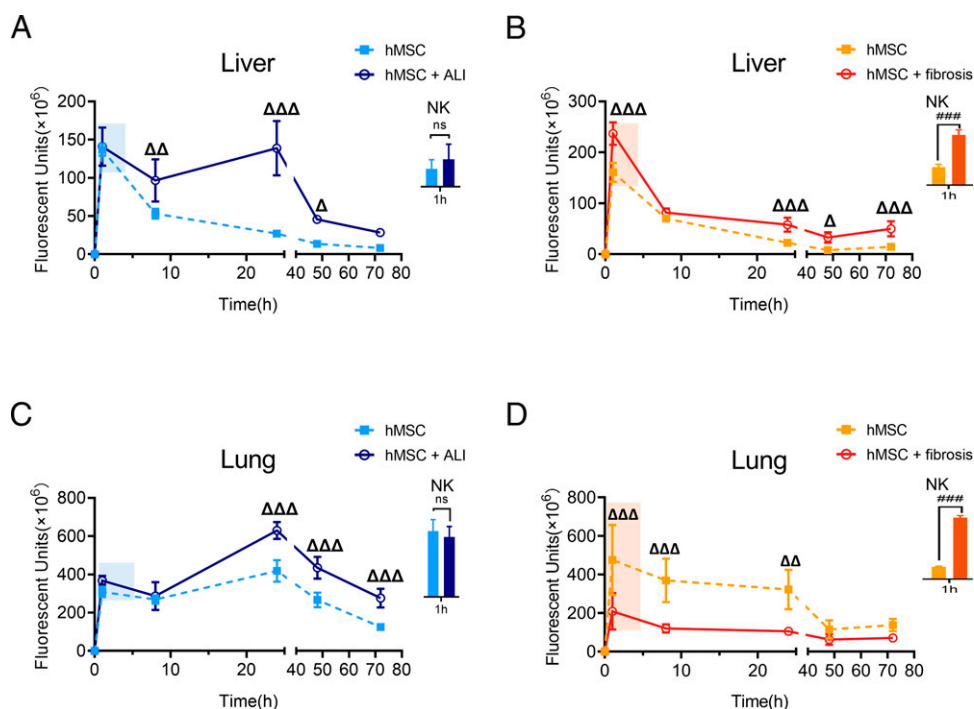
**Fig. 3.** The amount of hMSCs was both increased in the liver in two models but declined significantly in lung from CLF. (A–B) The fluorescence intensities-time curves in the liver were measured at 1, 8, 24, 48, and 72 hours after hMSCs injection in ALI or in the CLF model. (C–D) The fluorescence intensities-time curves in the lung of hMSCs in ALI or in CLF model. The percentages of CD49b^{+}Nkp46^{+} cells at 1 hour time point in liver and lung from two experiments were also listed. Data are shown as the mean ± S.D. ($n$ = 3–5 per group per time point; $^{\Delta}P < 0.05$, $^{\Delta\Delta}P < 0.01$, $^{\Delta\Delta\Delta}P < 0.001$ versus hourMSCs; $^{###}P < 0.001$ versus hourMSCs; ns, not significant).

**hMSCs Exposure in the Liver of ALI and CLF Mice Were Both Increased.** To find out the reason behind the divergent performance against liver injury in two liver injury models, we first compared the distribution of hMSCs (Supplemental Fig. 1, A and B). The fluorescent intensity of hMSCs in the ALI and CLF mice liver was increased significantly (Fig. 3, A and B). The result was confirmed by qPCR (Supplemental Fig. 2, B and D). The results indicated that the residence time of hMSC in the liver (MRT) was both extended significantly. The $AUC_{liver\ 0-72\ hour}$ was increased by 96.2% in the CLF, whereas the $AUC_{liver\ 0-72\ hour}$ increased by 177.1% in the ALI mice (Tables 1 and 2).

**hMSCs Exposure Was Increased in the Lung of ALI Mice, Whereas Decreased in CLF.** The divergent improvement of cell exposure in the liver could not fully explain the efficacy difference of hMSCs. Since the lung is the major site for MSC distribution and elimination, the change of MSC exposure in the lung was further investigated. In ALI mice, more injected MSC cells accumulated in the lung compared with healthy animals (Fig. 3C and Supplemental Fig. 2A). The $C_{max}$ and $AUC_{lung\ 0-72\ hour}$ increased by 50.5% and 51.1%, respectively (Table 1). Surprisingly, after a single administration of hMSCs, hMSCs accumulation in the lung decreased significantly in CLF animals (Fig. 3D and Supplemental Fig. 2C). The $C_{max}$ and $AUC_{lung\ 0-72\ hour}$ were reduced by nearly 57.5% and 60.7%, respectively (Table 2).

Since the majority of MSC injected was accumulated in the lung, not the liver ($AUC_{lung\ 0-72\ hour}$ was near 10-folds the value of $AUC_{liver\ 0-72\ hour}$), the overall reduced residence time of hMSCs in the lung of CLF was consistent with its limited efficacy after a single administration.

**NK Cells Were Downregulated in ALI but Activated in CLF Animals.** Next, we intended to find the possible explanation for the difference in the elimination process of hMSCs between the ALI and CLF models. Several studies have reported that NK cells are capable to lyse

MSCs in vitro (Aggarwal and Pittenger, 2005; Spaggiari et al., 2006; Götherström et al., 2011), and MSCs may also sacrifice because of NK cells-mediated lysis when circulating throughout the body. Therefore, we investigated whether the diverse NK alteration under different pathologic conditions, which have been reported in multiple studies (Liu et al., 2019; Salhab et al., 2020), may contribute to the MSC clearances in the two liver disease models. To further detect the percentage of NK cells in body, three biomarkers, CD49b (mature markers), CD107a (lysis marker), and Nkp46 (NK activating receptor) were employed (Alter et al., 2004; Walzer et al., 2007). The results showed that in ALI animals, the percentages of CD49b^{+}Nkp46^{+} cells were significantly decreased in the lung and liver (Fig. 4, A–C), which was consistent with the decreased fluorescence of Nkp46 and CD107a in the lung and liver (Supplemental Fig. 3, A and B). However, it was interesting to find that NK cells activity in the lung was upregulated in CLF (Fig. 4D and Supplemental Fig. 3C). The percentages of CD49b^{+}Nkp46^{+} cells in the lung were elevated approximately 2 to 5 times (Fig. 4D), further validated by immunofluorescence (Supplemental Fig. 3C). The percentage of hepatic NK cells was also detected (Fig. 4E and Supplemental Fig. 3D). The above data revealed a general negative correlation between NK cell activation and hMSCs exposure in mice. The upregulation of NK cells in tissues under diseases might lead to a greater loss of MSCs cells and vice versa.

**Depletion of NK Cells Enhanced the Exposure of hMSCs.** To verify the central role of NK cells in lysing MSCs, hMSCs were cocultured with IL-2 activated NK92 cells. Activated NK cells could efficiently lyse MSCs after 4 hours of coculture according to cytotoxicity assay (Supplemental Fig. 4B).

In the animal experiment, antiasialo GM-1 antibody was applied to deplete NK cells in Balb/c mice (Fig. 5, C and D and Supplemental Fig. 4A). As expected, the suppression of NK cells led to an enhanced exposure of hMSCs (Fig. 5, A and B). further validated by qPCR results

TABLE 1

Pharmacokinetic parameters of hMSCs in the lung and liver in $CCl_4$-induced acute liver injury mice

| | $T_{max}$ (h) | MRT (h) | $t_{1/2}$ (h) | $C_{max}$ (FU × $10^6$) | $AUC_{0-72\ h}$ (FU × h × $10^6$) |
|---|---|---|---|---|---|
| Liver | | | | | |
| hMSCs | 1 | 18.7 ± 0.9 | 27.5 ± 2.6 | 136.8 ± 7.8 | 2125.0 ± 83.1 |
| + ALI | 1 | 24.9 ± 3.4* | 22.4 ± 4.9 | 147.6 ± 31.3 | 5889.0 ± 580.9*** |
| Lung | | | | | |
| hMSCs | 24 | 30.9 ± 1.1 | 28.0 ± 4.2 | 418.5 ± 56.4 | 20588.0 ± 1068.0 |
| + ALI | 24 | 33.0 ± 4.7 | 41.6 ± 7.3** | 629.8 ± 43.9*** | 31100.0 ± 1450.0*** |

ALI, acute liver injury; AUC, area under the plasma concentration curve; $C_{max}$, peak concentration; FU, fluorescent units; MRT, mean residence time; $t_{1/2}$, the elimination half-life; $T_{max}$, peak time. Data are shown as the mean ± S.D. (*$P$ < 0.05, **$P$ < 0.01, ***$P$ < 0.001, versus hMSCs).

(Supplemental Fig. 2, E and F). For example, the fluorescent intensity of liver and lung at 1 hour after hMSCs injection in the NK-depleted group was increased by 71.9% and 135.9% respectively, compared with their counterparts in the control mice. Therefore, our results indicated that NK cells were at least partially responsible for eliminating exogenous MSCs in vitro and in vivo.

**PK Pattern of mMSCs in ALI was Comparable to hMSCs.** The exposure of mouse-derived MSCs were investigated in ALI animals. The mouse adipose-tissue derived MSCs were employed as research control to identify potential species difference.

The result indicated that mMSCs residence in the lung and liver was also significantly increased during ALF (Fig. 6, A and B). NK cells in the lung and liver were also remarkably decreased (Fig. 6, C and D). Those data implied that mMSCs cell fate was close to human-derived MSCs in the $CCl_4$-induced liver injury model (Fig. 3, A and C).

### Discussion

Mesenchymal stem cells have been widely investigated in diseases at preclinical studies. However, in a lot of scenarios, MSCs failed to show expected results in clinical trials (Galipeau and Sensebe, 2018). The main aim of this study was to supply an alternative explanation from the pharmacokinetic perspective. $CCl_4$ is a classic toxin, which could induce hepatic oxidative stress, inflammation response, and fibrosis (Weber et al., 2003; Torres et al., 2016; Zhang et al., 2017). $CCl_4$-induced ALI model is applied to reproduce acute liver injury or fulminant liver failure, whereas the CLF model could mimic human chronic liver fibrosis and cirrhosis. In this study, the ALI and CLF model were established by the same dose of $CCl_4$ with different administration frequencies. The purpose is to minimize the disturbances of potential variables, such as chemical agents, animal strains, and others (Liu et al., 2019; Ye et al., 2019). We have observed the homing of MSC in the liver of both models (the exposure of hMSCs in the liver of two models was significantly enhanced), consistent with previous literature (Karp and Leng Teo, 2009). However, when we explored the cell fate in tissues beyond the liver, a distinct difference in hMSCs

exposure in the lung was noticed between ALI and CLF animals. The activation or suppression of NK cells in different liver injury models might contribute to this distribution pattern of MSCs. The results indicate the exposure correlated with the extent of MSC hepatoprotective performance in the two models.

We wonder whether a single administration of hMSCs was able to protect the liver from inflammation in two representative models. In ALI mice, hMSCs significantly reduced the ALT and AST levels and the proinflammation gene expressions (Fig. 1, B and C), consistent with reported studies before (Shi et al., 2019). Whereas in CLF, although single hMSCs administration reduced ALT/AST levels, it showed limited efficacy against chronic hepatic and pulmonary fibrosis (Fig. 1, G and H; Fig. 2, B and C). Actually, it has been confirmed in previous reports that usually at least two repeated administrations of MSCs were required to attenuate liver fibrosis in CLF models (Ali et al., 2012; Luo et al., 2019). For example, the dosage regimen in one successful MSCs' treatment on decompensated liver cirrhosis required patients to receive MSCs transfusion once every 4 weeks three times (8 weeks in total) (Zhang et al., 2012).

The exposure of hMSCs in the liver of these two models was both significantly enhanced, but hMSCs had a greater increase in the $AUC_{liver\ 0-72\ hour}$ in ALI than CLF (177% versus 96.2%). The $AUC_{lung\ 0-72\ hour}$ of hMSCs also increased significantly in ALI lung (51.1%). However, in CLF mice, a surprisingly declined hMSCs exposure was noticed: the $AUC_{lung\ 0-72\ hour}$ and $C_{max}$ decreased by 60.7% and 57.5%, respectively (Table 2). The PK properties showed similar trends in the fluorescent detection and qPCR assays (Fig. 3 and Supplemental Fig. 2).

Therefore, the next question is why MSCs had opposite cell fates in the lung of ALI and CLF. It has been widely reported that MSCs possess a homing capacity. The inflammatory sites would release signals and attract transplanted MSCs into the injury sites (Leibacher and Henschler, 2016). In our CLF model, pulmonary pathology, like inflammation infiltration, alveolar fibrosis, and stale hemorrhage, were all observed (Fig. 2B). However, the accumulation of MSCs in the lung significantly decreased compared with the control (Fig. 3D). This phenomenon couldn't be explained by. the cell homing theory.

TABLE 2

Pharmacokinetic parameters of hMSCs in the lung and liver in $CCl_4$-induced chronic fibrosis mice

| | $T_{max}$ (h) | MRT (h) | $t_{1/2}$ (h) | $C_{max}$ (FU × $10^6$) | $AUC_{0-72\ h}$ (FU × h × $10^6$) |
|---|---|---|---|---|---|
| Liver | | | | | |
| hMSCs | 1 | 16.8 ± 0.7 | 20.0 ± 0.5 | 160.8 ± 18.8 | 2263.0 ± 89.6 |
| + fibrosis | 1 | 25.6 ± 2.1*** | 51.8 ± 21.0* | 237.0 ± 22.4*** | 4440.0 ± 337.7*** |
| Lung | | | | | |
| hMSCs | 2.8 ± 3.5 | 25.8 ± 2.0 | 36.7 ± 12.4 | 495.8 ± 151.0 | 16991.0 ± 2086.0 |
| + fibrosis | 2.4 ± 3.1 | 27.9 ± 4.3 | 68.4 ± 52.3 | 210.8 ± 93.2** | 6680.0 ± 669.1*** |

AUC, area under the plasma concentration curve; $C_{max}$, peak concentration; FU, fluorescent units; MRT, mean residence time; $t_{1/2}$, the elimination half-life; $T_{max}$, peak time. Data are shown as the mean ± S.D. (*$P$ < 0.05, **$P$ < 0.01, ***$P$ < 0.001, versus hMSCs).
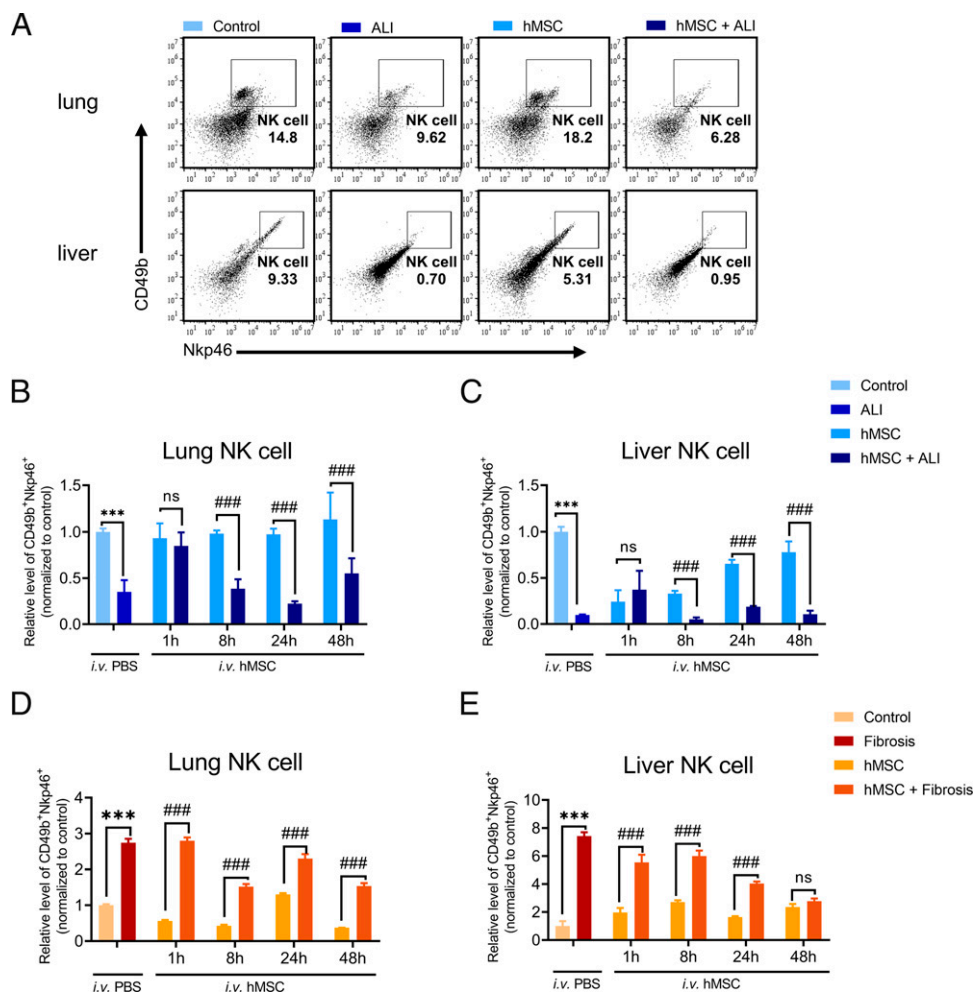
**Fig. 4.** NK cells were suppressed in ALI, although activated in the fibrotic lung and liver. (A) NK cells were analyzed by flow cytometry with PE-CD49b antibody and Dylight405-Nkp46 antibody. (B–C) Percentages of CD49b$^+$Nkp46$^+$ cells in the lung and liver lymphocytes in ALI experiment. (D–E) Quantitative analysis of NK cells in the lung and liver lymphocytes in CLF experiment. Data are shown as the mean ± S.D. ($n$ = 4 per group per time point; ***$P$ < 0.001, versus Con; $^{###}P$ < 0.01 versus hMSCs; ns, not significant).

NK cells are widely present in most mammal tissues, including lung, liver, spleen, and peripheral blood (Bjorkstrom et al., 2016; Cong and Wei, 2019). NK cells were reported to have critical roles in lysing hMSCs (Spaggiari et al., 2006). For exogenous MSCs, the low MHC-I expression and activating NK cell receptor ligands, like Poliovirus Receptor and MHC class I polypeptide-related sequence A, render it a susceptible target for NK cell-mediated lysis (Ej Reinders, 2014). The NK cell percentage in the lung of CLF animals increased 2–5 times compared with the control (Fig. 4D), which corresponded to the decreased hMSC cell exposure in the lung (Fig. 3D). On the contrary, in ALI animals, the percentage of NK cells was reduced in the lung (Fig. 4B), whereas hMSCs exposure increased (Fig. 3C). Interestingly, in the ALI experiment, there was no significant difference in the percentage of NK cells between animals with or without CCl$_4$ induction at the beginning of MSC administration (1 hour), which was consistent with the fact that MSCs concentration did not change immediately after administration in ALI (Figs. 3A and 4C).

The decrease of NK cells in ALI animals was consistent with the previous report (Liu et al., 2019). Whereas to our knowledge, the increase of NK cells in the lung of CLF animals has never been reported before. It is reasonable to speculate that the activation of NK cells was responsible for the accelerated elimination of MSCs in CLF mice lung. In the following study, NK cells were depleted with antiasialo GM1 antibody.

As expected, it brought a significantly greater accumulation in the lung and liver, which provided direct evidence for NK cell-mediated hMSC lysis (Fig. 5). The coculture systems also showed that hMSC were susceptible to the cytotoxicity of NK cells (Supplemental Fig. 4B).

In general, MSCs in the lung might be more susceptible to NK cells than in the liver. It was reported that in mice, lung NK cells account for about 10% of the lymphocytes, which was much higher than the percentages in other tissues, including liver (~6%) (Gregoire et al., 2007). Among them, the most mature and cytotoxic phenotype is CD27$^-$CD11b$^+$ NK cells, which are found at a higher frequency in the lung NK cells (>70%) than those in the liver (~30%) (Wang et al., 2012). It is reasonable to speculate that the total injected MSC amounts in lung of CLF animals decreased remarkably because of the activation of NK cells, since nearly 90% of transplanted MSCs accumulated in the lung (Han et al., 2021).

Our finding has novel clinic meanings as well. Firstly, the clinic dosage needs adjustment based on the NK cell activities in patients instead of simply adopting the dosage scaled up from preclinic studies or used in healthy volunteers. Besides, in many liver cirrhosis clinic trials, patients have to receive repeated MSCs injections (Shi et al., 2012; Miryounesi et al., 2013; Chen et al., 2014; Jang et al., 2014; Liao et al., 2020). Our results supplied an alternative rationale for why hMSC may not work in the clinic: the accelerated clearance of hMSC
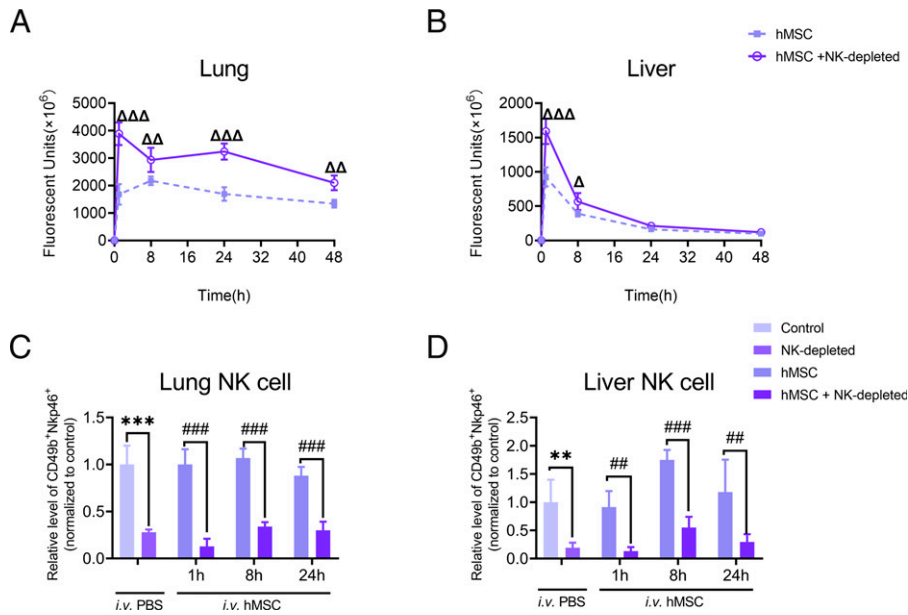
**Fig. 5.** Depletion of NK cells facilitated hMSCs residence. (A–B) The fluorescence intensities-time curve in the lung and liver were measured in NK-depleted mice 2 days after the intraperitoneal administration of 20 $\mu l$ anti-Asialo-GM1 antibody. (C–D) Quantification of NK cells in the lung and liver by flow cytometry. Data are shown as the mean ± S.D. ($n$ = 4–5 per group per time point; $^\Delta P < 0.05$, $^{\Delta\Delta} P < 0.01$, $^{\Delta\Delta\Delta} P < 0.001$ versus hourMSCs, $^{**} P < 0.01$, $^{***} P < 0.001$, versus Con; $^{\#\#} P < 0.01$, $^{\#\#\#} P < 0.001$ versus hMSCs).

in chronic liver fibrotic situations. The relationship between the PK variability, MSC efficacy, immune responses, and liver disease severity was linked in our study for the first time.

In this study, mouse adipose tissue-derived MSCs were employed to investigate if there is any species difference regarding the elimination pattern for MSCs under diseases compared with hMSCs. Higher mMSCs amounts and lower NK cell activities were found in the ALI mice, suggesting a similar kinetic pattern shared by human and mouse MSCs derived from different tissues (Fig. 6). These results suggested that it might be feasible to translate our preclinical findings into clinical studies but needs confirmation with more patient data. Our previous

work suggested mMSC PK patterns are very close to hMSCs in healthy mice (Han et al., 2021). Considering the similar behavior of mMSC and hMSC in ALI, it is reasonable to speculate that PK patterns of mMSCs in the CLF model are close to hMSCs as well. Anyway, the speculation needs to be validated in future work, especially in the clinic.

There were also some limitations of the present study. For example, the pharmacokinetic pattern of MSCs and the participation of NK cells-mediated elimination needs to be further explored in other disease models. It is necessary to estimate the contribution of other immune cells as well. The fluorescent intensity of hMSCs in lung showed some fluctuations in the ALI experiment (Fig. 3C). The phenomenon might be
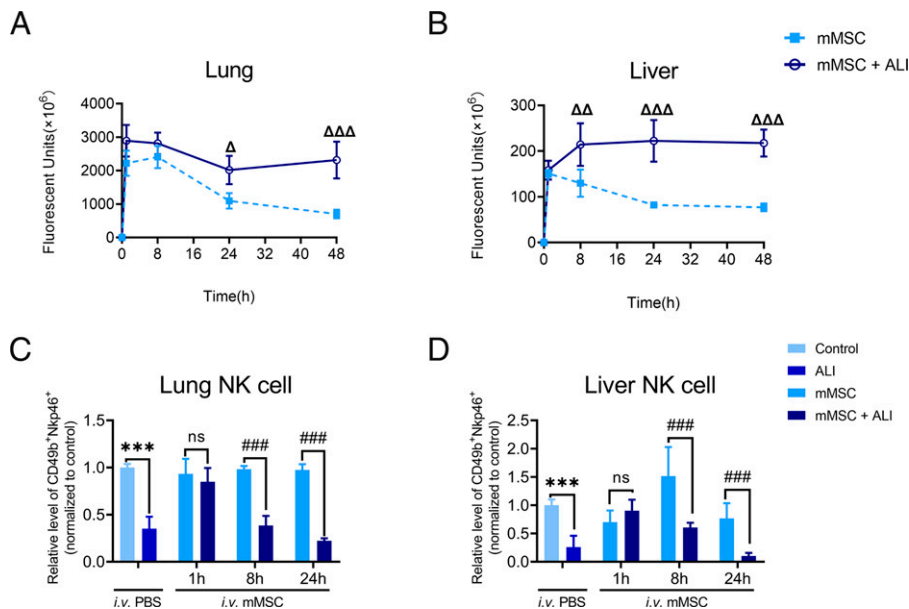


**Fig. 6.** mMSCs experienced a similar deposition process in ALI mice. (A–B) The fluorescence intensities-time curve in the lung and liver was measured at 1, 8, 24, and 48 hours after mMSCs injection in ALI. (C–D) Frequency of CD49b$^+$Nkp46$^+$ cells in lung lymphocytes and liver lymphocytes. ALI, acute liver injury. Data are shown as the mean ± S.D. ($n$ = 3–4 per group per time point; $^\Delta P < 0.05$, $^{\Delta\Delta} P < 0.01$, $^{\Delta\Delta\Delta} P < 0.001$ versus mMSCs, $^{**} P < 0.01$, $^{***} P < 0.001$, versus Con; $^{\#\#\#} P < 0.01$ versus mMSCs; ns, not significant).

attributed to machine distraction, as such increase was not observed in the parallel qPCR studies (Supplemental Fig. 2B). Anyway, this distraction will not change the conclusion of that study. Besides, we noticed the discrepancy between the gene and protein expression of α-sma (Fig. 1, G and J; Fig. 2C), one important fibrosis marker. This phenomenon was found in another report (Park et al., 2009) and our in-house data, but the potential explanation remains to be further explored.

In conclusion, this study revealed the differences between the distribution and efficacy of MSCs in ALI and CLF, which could partially explain by the divergent NK functions. To the best of our knowledge, it is the first time investigating the PK of MSCs under liver diseases. The distinct fates and efficacies of MSCs in acute liver injury or chronic fibrosis mice led to a comprehensive understanding of cell disposition and elimination. Our data suggested that the NK cell-associated MSCs clearance in lung instead of the liver could be critical to MSC's efficacy. Future studies will be warranted on these interesting questions to advance the application of MSCs in the clinic.

## Authorship Contributions

*Participated in research design:* C.H. Ma, Han, Tang, R. Huang, W. Huang, Pan.

*Conducted experiments:* C.H. Ma, Han, J. Wu, Deng, He, C. Ma.

*Performed data analysis:* C.H. Ma, Han, J. Wu, Z. Wu.

*Wrote or contributed to the writing of the manuscript:* C.H. Ma, Pan.

## Reference

Aggarwal S and Pittenger MF (2005) Human mesenchymal stem cells modulate allogeneic immune cell responses. *Blood* 105:1815–1822.

Ali G, Mohsin S, Khan M, Nasir GA, Shams S, Khan SN, and Riazuddin S (2012) Nitric oxide augments mesenchymal stem cell ability to repair liver fibrosis. *J Transl Med* 10:75.

Alter G, Malenfant JM, and Altfeld M (2004) CD107a as a functional marker for the identification of natural killer cell activity. *J Immunol Methods* 294:15–22.

Björkström NK, Ljunggren HG, and Michaëlsson J (2016) Emerging insights into natural killer cells in human peripheral tissues. *Nat Rev Immunol* 16:310–320.

Chen X, Gan Y, Li W, Su J, Zhang Y, Huang Y, Roberts AI, Han Y, Li J, Wang Y, et al. (2014) The interaction between mesenchymal stem cells and steroids during inflammation. *Cell Death Dis* 5:e1009.

Cong J and Wei H (2019) Natural killer cells in the lungs. *Front Immunol* 10:1416.

Creane M, Howard L, O'Brien T, and Coleman CM (2017) Biodistribution and retention of locally administered human mesenchymal stromal cells: quantitative polymerase chain reaction-based detection of human DNA in murine organs. *Cytotherapy* 19:384–394.

Daley GQ (2012) The promise and perils of stem cell therapeutics. *Cell Stem Cell* 10:740–749.

Ej Reinders M (2014) NK cells and MSCs: possible implications for MSC therapy in renal transplantation. *J Stem Cell Res Ther* 4:100016.

Estes BT, Diekman BO, Gimble JM, and Guilak F (2010) Isolation of adipose-derived stem cells and their induction to a chondrogenic phenotype. *Nat Protoc* 5:1294–1311.

Freud AG, Mundy-Bosse BL, Yu J, and Caligiuri MA (2017) The broad spectrum of human natural killer cell diversity. *Immunity* 47:820–833.

Galipeau J and Sensébé L (2018) Mesenchymal stromal cells: clinical challenges and therapeutic opportunities. *Cell Stem Cell* 22:824–833.

Götherström C, Lundqvist A, Duprez IR, Childs R, Berg L, andle Blanc K (2011) Fetal and adult multipotent mesenchymal stromal cells are killed by different pathways. *Cytotherapy* 13:269–278.

Grégoire C, Chasson L, Luci C, Tomasello E, Geissmann F, Vivier E, and Walzer T (2007) The trafficking of natural killer cells. *Immunol Rev* 220:169–182.

Han L, Ma C, Peng H, Wu Z, Xu H, Wu J, Zhang N, Jiang Q, Ma C, Huang R, et al. (2021) Define mesenchymal stem cell from its fate: biodisposition of human mesenchymal stem cells in normal and Con-A induced liver injury mice. *J Pharmacol Exp Ther* 379:125–133.

Han YF, Tao R, Sun TJ, Chai JK, Xu G, and Liu J (2013) Optimization of human umbilical cord mesenchymal stem cell isolation and culture methods. *Cytotechnology* 65:819–827.

Jang YO, Kim YJ, Baik SK, Kim MY, Eom YW, Cho MY, Park HJ, Park SY, Kim BR, Kim JW, et al. (2014) Histological improvement following administration of autologous bone marrow-derived mesenchymal stem cells for alcoholic cirrhosis: a pilot study. *Liver Int* 34:33–41.

Karp JM and Leng Teo GS (2009) Mesenchymal stem cell homing: the devil is in the details. *Cell Stem Cell* 4:206–216.

Leibacher J and Henschler R (2016) Biodistribution, migration and homing of systemically applied mesenchymal stem/stromal cells. *Stem Cell Res Ther* 7:7.

Liao N, Shi Y, Wang Y, Liao F, Zhao B, Zheng Y, Zeng Y, Liu X, and Liu J (2020) Antioxidant preconditioning improves therapeutic outcomes of adipose tissue-derived mesenchymal stem cells through enhancing intrahepatic engraftment efficiency in a mouse liver fibrosis model. *Stem Cell Res Ther* 11:237.

Liu J, Feng B, Xu Y, Zhu J, Feng X, Chen W, Sheng X, Shi X, Pan Q, Yu J, et al. (2019) Immunomodulatory effect of mesenchymal stem cells in chemical-induced liver injury: a high-dimensional analysis. *Stem Cell Res Ther* 10:262.

Luo XY, Meng XJ, Cao DC, Wang W, Zhou K, Li L, Guo M, and Wang P (2019) Transplantation of bone marrow mesenchymal stromal cells attenuates liver fibrosis in mice by regulating macrophage subtypes. *Stem Cell Res Ther* 10:16.

Miryounesi M, Piryaei A, Pournasr B, Aghdami N, and Baharvand H (2013) Repeated versus single transplantation of mesenchymal stem cells in carbon tetrachloride-induced liver injury in mice. *Cell Biol Int* 37:340–347.

Mohamadnejad M, Alimoghaddam K, Bagheri M, Ashrafi M, Abdollahzadeh L, Akhlaghpoor S, Bashtar M, Ghavamzadeh A, and Malekzadeh R (2013) Randomized placebo-controlled trial of mesenchymal stem cell transplantation in decompensated cirrhosis. *Liver Int* 33:1490–1496.

Pääkkö P, Anttila S, Sormunen R, Ala-Kokko L, Peura R, Ferrans VJ, and Ryhänen L (1996) Biochemical and morphological characterization of carbon tetrachloride-induced lung fibrosis in rats. *Arch Toxicol* 70:540–552.

Park O, Jeong WI, Wang L, Wang H, Lian ZX, Gershwin ME, and Gao B (2009) Diverse roles of invariant natural killer T cells in liver injury and fibrosis induced by carbon tetrachloride. *Hepatology* 49:1683–1694.

Poggi A, Prevosto C, Massaro AM, Negrini S, Urbani S, Pierri I, Saccardi R, Gobbi M, and Zocchi MR (2005) Interaction between human NK cells and bone marrow stromal cells induces NK cell triggering: role of NKp30 and NKG2D receptors. *J Immunol* 175:6352–6360.

Salhab A, Amer J, Yinying L, and Safadi R (2020) 25(OH) D3 alleviate liver NK cytotoxicity in acute but not in chronic fibrosis model of BALB/c mice due to modulations in vitamin D receptor. *BMC Gastroenterol* 20:102.

Schindelin J, Arganda-Carreras I, Frise E, Kaynig V, Longair M, Pietzsch T, Preibisch S, Rueden C, Saalfeld S, Schmid B, et al. (2012) Fiji: an open-source platform for biological-image analysis. *Nat Methods* 9:676–682.

Shi M, Zhang Z, Xu R, Lin H, Fu J, Zou Z, Zhang A, Shi J, Chen L, Lv S, et al. (2012) Human mesenchymal stem cell transfusion is safe and improves liver function in acute-on-chronic liver failure patients. *Stem Cells Transl Med* 1:725–731.

Shi X, Liu J, Chen D, Zhu M, Yu J, Xie H, Zhou L, Li L, and Zheng S (2019) MSC-triggered metabolomic alterations in liver-resident immune cells isolated from CCl₄-induced mouse ALI model. *Exp Cell Res* 383:111511.

Shim G, Lee S, Han J, Kim G, Jin H, Miao W, Yi TG, Cho YK, Song SU, and Oh YK (2015) Pharmacokinetics and in vivo fate of intra-articularly transplanted human bone marrow-derived clonal mesenchymal stem cells. *Stem Cells Dev* 24:1124–1132.

Spaggiari GM, Capobianco A, Becchetti S, Mingari MC, and Moretta L (2006) Mesenchymal stem cell-natural killer cell interactions: evidence that activated NK cells are capable of killing MSCs, whereas MSCs can inhibit IL-2-induced NK-cell proliferation. *Blood* 107:1484–1490.

Taslidere E, Esrefoglu M, Elbe H, Cetin A, and Ates B (2014) Protective effects of melatonin and quercetin on experimental lung injury induced by carbon tetrachloride in rats. *Exp Lung Res* 40:59–65.

Torres LR, Santana FC, Torres-Leal FL, Melo IL, Yoshime LT, Matos-Neto EM, Seelaender MC, Araújo CM, Cogliati B, and Mancini-Filho J (2016) Pequi (Caryocar brasiliense Camb.) almond oil attenuates carbon tetrachloride-induced acute hepatic injury in rats: Antioxidant and anti-inflammatory effects. *Food Chem Toxicol* 97:205–216.

Walzer T, Bléry M, Chaix J, Fuseri N, Chasson L, Robbins SH, Jaeger S, André P, Gauthier L, Daniel L, et al. (2007) Identification, activation, and selective in vivo ablation of mouse NK cells via NKp46. *Proc Natl Acad Sci USA* 104:3384–3389.

Wang J, Li F, Zheng M, Sun R, Wei H, and Tian Z (2012) Lung natural killer cells in mice: phenotype and response to respiratory infection. *Immunology* 137:37–47.

Weber LW, Boll M, and Stampfl A (2003) Hepatotoxicity and mechanism of action of haloalkanes: carbon tetrachloride as a toxicological model. *Crit Rev Toxicol* 33:105–136.

Wysoczynski M, Khan A, and Bolli R (2018) New paradigms in cell therapy: repeated dosing, intravenous delivery, immunomodulatory actions, and new cell types. *Circ Res* 123:138–158.

Xu T, Zhang Y, Chang P, Gong S, Shao L, and Dong L (2018) Mesenchymal stem cell-based therapy for radiation-induced lung injury. *Stem Cell Res Ther* 9:18.

Yang X, Meng Y, Han Z, Ye F, Wei L, and Zong C (2020) Mesenchymal stem cell therapy for liver disease: full of chances and challenges. *Cell Biosci* 10:123.

Ye Z, Lu W, Liang L, Tang M, Wang Y, Li Z, Zeng H, Wang A, Lin M, Huang L, et al. (2019) Mesenchymal stem cells overexpressing hepatocyte nuclear factor-4 alpha alleviate liver injury by modulating anti-inflammatory functions in mice. *Stem Cell Res Ther* 10:149.

Zhang DG, Zhang C, Wang JX, Wang BW, Wang H, Zhang ZH, Chen YH, Lu Y, Tao L, Wang JQ, et al. (2017) Obeticholic acid protects against carbon tetrachloride-induced acute liver injury and inflammation. *Toxicol Appl Pharmacol* 314:39–47.

Zhang Z, Lin H, Shi M, Xu R, Fu J, Lv J, Chen L, Lv S, Li Y, Yu S, et al. (2012) Human umbilical cord mesenchymal stem cells improve liver function and ascites in decompensated liver cirrhosis patients. *J Gastroenterol Hepatol* 27:112–120.

Zhao K, Lin R, Fan Z, Chen X, Wang Y, Huang F, Xu N, Zhang X, Zhang X, Xuan L, et al. (2022) Mesenchymal stromal cells plus basiliximab, calcineurin inhibitor as treatment of steroid-resistant acute graft-versus-host disease: a multicenter, randomized, phase 3, open-label trial. *J Hematol Oncol* 15:22.

Zhao L, Chen S, Shi X, Cao H, and Li L (2018) A pooled analysis of mesenchymal stem cell-based therapy for liver disease. *Stem Cell Res Ther* 9:72.

Zhong L, Yang M, Zou X, Du T, Xu H, and Sun J (2020) Human umbilical cord multipotent mesenchymal stromal cells alleviate acute ischemia-reperfusion injury of spermatogenic cells via reducing inflammatory response and oxidative stress. *Stem Cell Res Ther* 11:294.

**Address correspondence to**: Wei Huang, Shanghai Institute of Materia Medica, Chinese Academy of Sciences, Haike Road 501, Shanghai 201203, China. E-mail: huangwei@simm.ac.cn; Ruimin Huang, Shanghai Institute of Materia Medica, Chinese Academy of Sciences, Haike Road 501, Shanghai 201203, China. E-mail: rmhuang@simm.ac.cn; or Prof. Guoyu Pan, Shanghai Institute of Materia Medica, Chinese Academy of Sciences, Haike Road 501, Shanghai 201203, China. E-mail: gypan@simm.ac.cn